Letter

Multivalued dispersion equation for coupling between plasmons and surface optical phonons in a graphene/polar-substrate system

S. M. Kukhtaruk [1,*] and V. A. Kochelap [1,2]

[1]*Department of Theoretical Physics, V. Ye. Lashkaryov Institute of Semiconductor Physics, NASU, 03028 Kyiv, Ukraine*

[2]*CENTERA Laboratories, Institute of High Pressure Physics PAS, 01-142 Warsaw, Poland*

(Received 24 July 2024; revised 9 October 2024; accepted 19 November 2024; published 6 December 2024)

Dispersion equations are a common paradigm of collective excitation physics. However, in some systems, dispersion equations contain multivalued functions and their solutions are ambiguous. As an example, we consider graphene on a polar substrate where Dirac plasmons are coupled with surface optical phonons. The dispersion equation for this system contains square-root singularity. Using the initial value problem resolves this uncertainty and gives a unique solution. Particularly, we found that the lower plasmon-phonon mode, which in terms of dispersion can have a good quality factor, is almost absent in excitation spectra. The physical reason and experimental evidence of the mode collapse are discussed.

DOI: 10.1103/PhysRevB.110.L241403

Dispersion equations and relations are the key subjects of any linear theories that involve waves and collective excitations. One can find examples in the theories of plasmons [1–3], acoustic and optical phonons [4,5], magnons [6], polaritons [7], etc. In the case of the semiclassical theory of collective excitations of electron gas based on Boltzmann-Vlasov and Poisson equations, their coordinate and frequency Fourier transforms lead directly to the dispersion equation as the condition for the existence of nontrivial solutions of the system. Quantum theories (e.g., random phase approximation) give the ability to consider higher values of wave numbers and frequencies, to include purely quantum effects (e.g., interband transitions), and also lead to the analysis of dispersion equations. In both semiclassical and quantum theories the dispersion equations can be presented as zeros of dielectric function $\varepsilon(\omega, k)$, where ω and k are the frequency and wave number.

Usually $\varepsilon(\omega, k)$ includes an improper integral. To handle this problem, Landau [8] proposed to use the Laplace transform for the time variable instead of the Fourier transform. This approach corresponds to the formulation of the relevant initial value problem and resulted, particularly, in the discovery of the Landau damping effect. Nevertheless, in most cases, the Fourier transform and its consequence—the dispersion equation—can lead to the same result for collective excitations as the Laplace transform, if one adds a small imaginary part to the frequency, i.e., $\omega \to \omega + i0$ (see, e.g., Ref. [1]). The dispersion equation approach with such a regularization rule becomes widely used in the theoretical physics and spreads far beyond the collective excitation theory of electron plasma.

In this Letter, we show that the approach to the dispersion equation based on $\varepsilon(\omega, k) = 0$ cannot be applicable if the function $\varepsilon(\omega, k)$ contains the branch points. Particularly, we considered the excitation of the plasmons in graphene on a polar substrate and analyzed a strong coupling between plasmons in graphene and surface optical (SO) phonons of the substrate. It is known that the dielectric function for the Dirac electrons has branch points at $\omega = \pm v_F k$ with v_F being the Fermi velocity [9–13]. Thus, formal solutions of the dispersion equation depend on chosen branch cuts in the complex ω plane. To handle the problem we use the above-mentioned initial value problem. By this approach, we show that the coupling of plasmons and SO phonons affects pole and branch cut contributions, providing that the total contribution is unambiguous, i.e., it is independent of chosen branch cuts. Furthermore, we found that the hybrid plasmon-phonon mode, which in terms of standard dispersion is characterized by a good quality factor, actually collapses at $k \sim \omega_{\mathrm{TO}}/v_F$, where ω_{TO} is the frequency of transverse optical phonon of the substrate. Note, the evidence of the collapse can be seen in the relevant experiments [14,15].

The plasmon-SO phonon coupling in graphene was studied in a series of theoretical [16–20] and experimental [14,15,21–27] work by different methods. Moreover, graphene plasmonics and its potential applications were discussed in the recent reviews [28–33]. To the best of our knowledge, the effect of the collapse was not recognized and discussed.

Let us consider the graphene sheet, which is located at the coordinate $z = 0$ in the x-y plane on a polar substrate. We describe the electron subsystem by the distribution function $F(\mathbf{r}, \mathbf{p}, t)$, which is presented as $F(\mathbf{r}, \mathbf{p}, t) = F_0(\mathbf{p}) + \mathcal{F}(\mathbf{r}, \mathbf{p}, t)$. Here, $\mathbf{r}$ and $\mathbf{p}$ are two-dimensional (2D) vectors of the electron coordinate and momentum in the graphene sheet, $F_0(\mathbf{p})$ is the equilibrium Fermi distribution, and $\mathcal{F}(\mathbf{r}, \mathbf{p}, t)$

*Contact author: kukhtaruk@gmail.com

Published by the American Physical Society under the terms of the Creative Commons Attribution 4.0 International license. Further distribution of this work must maintain attribution to the author(s) and the published article's title, journal citation, and DOI.

is governed by the Boltzmann-Vlasov collisionless transport equation:

$$\frac{\partial \mathcal{F}}{\partial t} + v_F \frac{\mathbf{p}}{p}\frac{\partial \mathcal{F}}{\partial \mathbf{r}} - e\mathbf{E}_\parallel\Big|_{z=0}\frac{\partial F_0}{\partial \mathbf{p}} = 0, \tag{1}$$

where e is the elementary charge, and $\mathbf{E}_\parallel(\mathbf{r}, z, t)$ is the lateral component of the electric field $\mathbf{E}(\mathbf{r}, z, t) = (\mathbf{E}_\parallel, E_z)$ [34], which is given by the Poisson equation:

$$\nabla[\mathbf{E}+4\pi\mathbf{P}\,\theta(-z)] = -4\pi e\,\delta(z)\int\frac{g\,d^2p}{(2\pi\hbar)^2}\mathcal{F}(\mathbf{r}, \mathbf{p}, t). \tag{2}$$

Here, $\theta(-z)$ is the Heaviside step function, accounting for vacuum (polar substrate) under (below) the graphene. $\mathbf{P}(\mathbf{r}, z, t)$ is the substrate polarization, and factor $g = 4$ stands for the spin and valley degeneracies [11].

The polarization is determined by the optical displacements $\mathbf{w}(\mathbf{r}, z, t)$ of substrate ions and the total electric field: $\mathbf{P} = b_{12}\mathbf{w} + b_{22}\mathbf{E}$. The equation for displacements reads [35]

$$\frac{\partial^2 \mathbf{w}}{\partial t^2} + \gamma_{\mathrm{TO}}\frac{\partial \mathbf{w}}{\partial t} + \omega_{\mathrm{TO}}^2\mathbf{w} = b_{12}\mathbf{E}, \tag{3}$$

where coefficients $b_{12} = \sqrt{(\kappa_0 - \kappa_\infty)/4\pi}(\omega_{\mathrm{TO}})$ and $b_{22} = (\kappa_\infty - 1)/4\pi$. Parameters κ_0 and κ_∞ are static and high-frequency dielectric constants of the substrate, respectively; γ_{TO} is damping of transverse optical phonons.

Below we will use the scalar potential $\Phi(\mathbf{r}, z, t)$ instead of the field: $\mathbf{E}(\mathbf{r}, \mathbf{z}, \mathbf{t}) = -\nabla\Phi(\mathbf{r}, z, t)$. We perform the spatial Fourier transform for all spatially dependent quantities in the graphene sheet, e.g.,

$$\mathcal{F}(\mathbf{r}, \mathbf{p}, t) = \int d^2k\mathcal{F}_{\mathbf{k}}(\mathbf{p}, t)e^{i\mathbf{kr}}, \tag{4}$$

thus introduce $\Phi_{\mathbf{k}}(z, t)$, $\mathbf{P}_{\mathbf{k}}(z, t)$, and $\mathbf{w}_{\mathbf{k}}(z, t)$. For the obtained time-dependent system of equations the initial value problem can be formulated and solved using the Laplace transform

$$f_{\omega,\mathbf{k}}(\mathbf{p}) = \int_0^\infty dt\mathcal{F}_{\mathbf{k}}(\mathbf{p}, t)e^{i\omega t}, \tag{5}$$

$$\mathcal{F}_{\mathbf{k}}(\mathbf{p}, t) = \int_{-\infty+i\sigma}^{\infty+i\sigma}\frac{d\omega}{2\pi}f_{\omega,\mathbf{k}}(\mathbf{p})e^{-i\omega t}, \tag{6}$$

with $\sigma > 0$, i.e., the integration should be performed at the upper half plane of complex $\omega = \omega' + i\omega''$, higher than any singularities of $f_{\omega,\mathbf{k}}(\mathbf{p})$ [36]. Similarly, we introduce other Fourier-Laplace components: $\phi_{\omega,\mathbf{k}}(z)$, $\mathbf{P}_{\omega,\mathbf{k}}(z)$, and $\mathbf{w}_{\omega,\mathbf{k}}(z)$.

The final result for the Fourier-Laplace components of the distribution function and potential at the graphene sheet [37] are

$$f_{\omega,\mathbf{k}}(\mathbf{p}) = i\frac{\delta\mathcal{F}_{\mathbf{k}}^0(\mathbf{p}) - ie\phi_{\omega,\mathbf{k}}(0)\mathbf{k}\,dF_0(\mathbf{p})/d\mathbf{p}}{\omega - v_F\mathbf{kp}/p}, \tag{7}$$

$$\phi_{\omega,\mathbf{k}}(0) = \frac{\delta\phi^{el}(\omega, \mathbf{k}) + \delta\phi^{ph}(\omega, \mathbf{k})}{\varepsilon(\omega, k)}. \tag{8}$$

Here, we introduce functions

$$\delta\phi^{el}(\omega, \mathbf{k}) = -\frac{2\pi ie}{\kappa_\infty^* k}\int\frac{gd^2p}{(2\pi\hbar)^2}\frac{\left(\omega^2 - \omega_{\mathrm{TO}}^2 + i\gamma_{\mathrm{TO}}\omega\right)\delta\mathcal{F}_{\mathbf{k}}^0(\mathbf{p})}{\omega - v_F\mathbf{kp}/p}, \tag{9}$$

$$\delta\phi^{ph}(\omega, \mathbf{k}) = \frac{2\pi b_{12}}{\kappa_\infty^* k}\int_{-\infty}^0 dz\left(i\mathbf{k}\mathbf{W}_{\mathbf{k},\parallel}^0 - kW_{k,z}^0\right)e^{kz}, \tag{10}$$

which are defined by the Fourier components of the initial electron distribution function, $\delta\mathcal{F}_{\mathbf{k}}^0(\mathbf{p})$, and initial conditions of optical displacements, since $\mathbf{W}_{\mathbf{k}}^0 = \frac{\partial \mathbf{w}_{\mathbf{k}}}{\partial t}|_{t=0} - i(\omega + i\gamma_{\mathrm{TO}})\mathbf{w}_{\mathbf{k}}|_{t=0}$. In Eqs. (9) and (10) we introduce the parameter $\kappa_\infty^* = (\kappa_\infty + 1)/2$.

Consider the Fourier-Laplace component of the potential in the graphene layer given by Eq. (8). The dielectric function in this equation is

$$\varepsilon(\omega, k) = \left(\omega^2 - \omega_{\mathrm{SO}}^2 + i\gamma_{\mathrm{TO}}\omega\right)[1 - V(k)\Pi(\omega, k)] - (\omega_{\mathrm{SO}}^2 - \omega_{\mathrm{TO}}^2)V(k)\Pi(\omega, k), \tag{11}$$

where $\omega_{\mathrm{SO}} = \sqrt{(1+\kappa_0)/(1+\kappa_\infty)}\,\omega_{\mathrm{TO}}$ is the frequency of the SO phonon, $V(k) = 2\pi e^2/\kappa_\infty^* k$ is the Fourier transform of the Coulomb potential, and $\Pi(\omega, k)$ is graphene polarizability [9–12],

$$\Pi(\omega, k) = \frac{gk_BT}{2\pi\hbar^2 v_F^2}\ln\left[\exp\left(\frac{E_F}{k_BT}\right)+1\right]\left(\frac{\omega}{\sqrt{\omega^2 - v_F^2k^2}} - 1\right). \tag{12}$$

Expectedly, the considered potential is defined by the numerator, which depends on electron and phonon initial conditions, and the denominator, which depends on the dielectric function (11). Equation $\varepsilon(\omega, k) = 0$ has a typical structure of a dispersion equation for coupled subsystems. Indeed, the first two brackets give the dispersion relations of uncoupled SO phonons and plasmons, and the last term represents the coupling between them. The same dispersion equation can be obtained using a standard approach based on Fourier transform, resulting in zero of the determinant of homogeneous system of equations.

The polarizability (12) is the double valued function with two branch points, $\omega = \pm v_F k$. So far, it is defined in the upper half plane of ω, as well as all ω-dependent quantities [see Eq. (6)]. For what follows we extend the definition of these functions to the lower half plane of ω, where, for instance, zeros of the dielectric function are expected. For this, one needs to introduce the branch cuts and perform the analytical continuation in such a way that any ω-dependent function should be continuous everywhere in the ω plane, except poles and except branch cuts, where the function must undergo a jump in its value (see Supplemental Material for details [37]). We stress that integral (6) and similar integrals for other Laplace components converge if all singularities of integrands are below the line $\omega'' = \sigma$, which is required by the conditions of Laplace transform [36]. This implies that any branch cut(s) below this line do not affect the convergence of the integrals. Therefore, there are many possibilities in choosing the branch cuts. Further, we will consider two types of branch cuts that are most convenient for further analytical calculations (see Ref. [37] for details).

Figure 1(a) shows the branch cut on the ω plane, which is defined as the segment at the real axis, i.e., $-v_F k \leqslant \omega' \leqslant v_F k$. We refer to this branch cut as BC-I. The corresponding

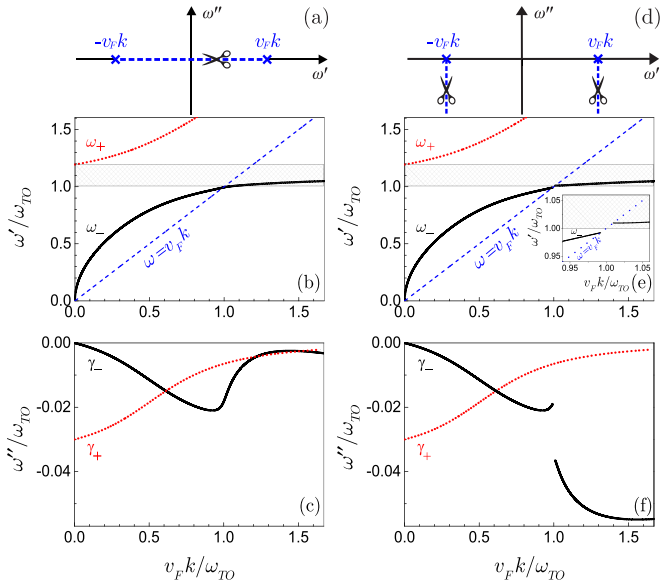


FIG. 1. The branch cuts BC-I (a) and BC-II (d) on the complex ω planes. Frequencies [(b), (e)] and decrements [(c), (f)] of joint plasmon-SO phonon oscillations, which correspond to BC-I (left panel) and BC-II (right panel). The inset in (e) shows a magnified view near $\omega' \approx v_F k$. Parameters for graphene on the SiC substrate are as follows: electron concentration and temperature are $n_0 = 2 \times 10^{12}$ cm^{-2} and $T = 300$ K; static and high-frequency dielectric constants for SiC are $\kappa_0 = 9.72$ and $\kappa_\infty = 6.52$; $\omega_{\rm TO} = 2\pi \times 23.9$ THz, and $\gamma_{\rm TO} = 0.06\,\omega_{\rm TO}$ [20,38].

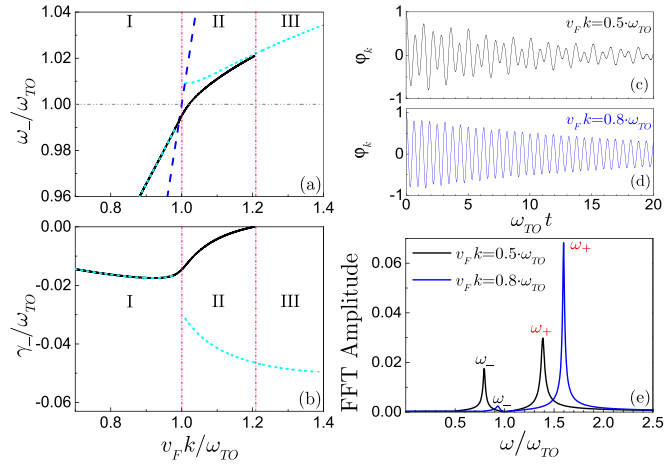


FIG. 2. (a) Frequency and (b) decrement of the ω_- mode, obtained for the same parameters as Fig. 1 except $\gamma_{\rm TO} = 0.05\,\omega_{\rm TO}$. The $\omega - k$ plane is divided into three areas, where (A-I) solutions coincide for both types of branch cuts, (A-II) branch ω_- exists for both BC-I and BC-II, and (A-III) solution exists only for BC-II. (c and d) Two signals and (e) their spectral FFT amplitudes for $v_F k = 0.5\,\omega_{\rm TO}$ and $v_F k = 0.8\,\omega_{\rm TO}$, respectively.

solutions of the dispersion equation, i.e., zeros of the dielectric function (11), shown in Figs. 1(b) and 1(c), are for real and imaginary parts of ω, respectively. Figure 1(b) shows a well-visible avoided crossing, which corresponds to hybridized plasmon-SO phonon modes, ω_+ and ω_-. Corresponding decrements, γ_+ and γ_-, are shown in Fig. 1(c). At small wave numbers, the branch ω_+ starts from $\omega_{\rm SO}$ with damping $\gamma_+ = \gamma_{\rm TO}/2$. While the branch ω_- starts from the plasmon $\sqrt{k}$ dispersion with zero Landau damping for 2D Dirac electrons (see, e.g., Ref. [16]). The branch ω_+ is always higher than the line $\omega = v_F k$, and thus its decrement monotonically decreases with increasing of the wave number. The branch ω_- is continuous and crosses the line $\omega = v_F k$, while behavior of the decrement γ_- is strongly nonmonotonic.

Now, let us consider the branch cuts, which are shown in Fig. 1(d). These are two cuts along the semi-infinite lines in the lower half of the ω plane, $\omega = \pm v_F k + i\omega''$ with $\omega'' \leqslant 0$ (BC-II). The corresponding solutions of the dispersion equation are shown in Figs. 1(e) and 1(f). While the branch ω_+ is exactly the same as in Fig. 1(b) with the same damping decrement γ_+ as in Fig. 1(c), the branch ω_- now possesses a small gap near the line $\omega = v_F k$. This region is magnified in the inset of Fig. 1(e). The size of the gap increases with increasing plasmon-SO phonon coupling, which can be enlarged by increasing the electron concentration and larger for greater difference between κ_0 and κ_∞. The decrements in Figs. 1(c) and 1(f) are even more different: for the latter case, ω'' has a final gap, and in the region $\omega < v_F k$, the hybrid plasmon-SO phonon mode for BC-I has a high-quality factor, while it has a low-quality factor for BC-II.

The contradiction of the results obtained for two different branch cuts becomes even more strong if we slightly decrease the phonon damping. Figures 2(a) and 2(b) illustrate this for the decrease in the damping by 20%, $\gamma_{\rm TO} = 0.05\,\omega_{\rm TO}$. Figure 2(a) shows the ω_- branch for the branch cuts BC-I and BC-II (black solid and cyan dotted lines, respectively). Here, one can see that the branch ω_- suddenly disappears for $v_F k \gtrsim 1.2\,\omega_{\rm TO}$ for the case of BC-I. For this branch cut, the decrement γ_- in Fig. 1(c) moves upward as a function of the wave number and eventually touches zero simultaneously with the disappearance of the ω' solution. Unusual behavior of $\omega_-(k)$ near $\omega = v_F k$ was noted in previous works: disappearing of the ω_- branch was discovered in Ref. [16]; the gap in $\omega_-(k)$ dependence for BC-II was also found in Ref. [19]. Such contradictions between dispersion relations are nonphysical. We argue that sets of dispersion curves, particularly presented in Figs. 1 and 2, do not give a full picture of oscillations in the system. Here, we show that mathematically correct accounting of any branch cuts gives the unambiguous solution, which is our main statement.

To prove the main statement, we note that all Fourier-Laplace components, such as $f_{\omega,\mathbf{k}}$ and $\phi_{\omega,\mathbf{k}}(z)$, enter the integrals similar to (6). For instance, the final solution for the Fourier component of the potential consists of, in general, three contributions: poles contribution, branch cut(s) contribution, and all other contributions that can be generated by an initial distribution function (e.g., van Kampen's waves [12,39]). While all these distinct components depend on the branch cuts, we argue that their sum (the total contribution) is *unambiguous*. Indeed, contributions from poles, branch cuts, etc. arise as a result of deformation of integration contours and respective analytical continuation of integrands defined at $\omega'' \geqslant \sigma > 0$. For the latter inequalities, the values of $\sqrt{\omega^2 - v_F^2 k^2}$ are the same for any possible branch cuts [36,37]. Therefore, any correct analytical continuation of

Laplace components to region $\omega'' < \sigma$ should give the same final result, despite the particular contributions being different and depending on branch cuts.

Before proceeding with further analysis, let us consider the limitations of the model and estimate the parameters. The collisionless transport equation is valid if $\omega\tau_p \gg 1$ and $kl_p \gg 1$, where τ_p is the characteristic scattering time and $l_p = v_F\tau_p$ is the carrier mean free path. At room temperature and the concentration, $n_0 = 2\times10^{12}$ cm^{-2}, Fermi energy $E_F \approx 160$ meV, and electron mobility for graphene on SiC $\mu \sim 1000$ cm^2/Vs [40]. The simple phenomenological estimation gives $\tau_p \approx \mu E_F/ev_F^2 = 0.16$ ps. For the characteristic frequency $\omega = \omega_{\rm TO}$ and wave number $k = \omega_{\rm TO}/v_F$, we have $\omega_{\rm TO}\tau_p \approx kl_p \approx 24 \gg 1$. We consider n-doped graphene and restrict ourselves to excitations with ω and k for which the interband processes can be neglected. Such an approach is valid for $\hbar\omega < E_F$ and $\hbar k < p_F$ at $k_BT \ll E_F$, where $p_F = \hbar\sqrt{\pi n_0}$ is the Fermi momentum. For the mentioned parameters, we find $E_F/(\hbar\omega_{\rm TO}) \approx 1.6$ and $v_F p_F/(\hbar\omega_{\rm TO}) \approx 1.67$, which explains the ranges of ω and k shown in Fig. 1.

To demonstrate the main features of the coupled system, further, we assume the isotropic initial electron distribution [i.e., $\delta\mathcal{F}^0_{\mathbf{k}}(\mathbf{p}) = \delta\mathcal{F}^0_{\mathbf{k}}(p)$], and zero initial conditions for phonons [i.e., such that $\delta\phi^{ph}(\omega,\mathbf{k}) = 0$], which are close to the experimental conditions [14,15]. In this case, the potential at $t = 0$ is given by

$$\Phi^0_k(0) = -\frac{eg}{\kappa^*_\infty\hbar^2 k}\int_0^\infty dpp\,\delta\mathcal{F}^0_{\mathbf{k}}(p). \tag{13}$$

It is convenient to introduce the normalized potential $\varphi_{\mathbf{k}}(t) = \Phi_{\mathbf{k}}/\Phi^0_k$:

$$\varphi_{\mathbf{k}}(t) = \frac{i}{2\pi}\int_{-\infty+i\sigma}^{\infty+i\sigma} d\omega\,\frac{\omega^2-\omega^2_{\rm TO}+i\gamma_{\rm TO}\omega}{\varepsilon(\omega,k)\sqrt{\omega^2-v_F^2k^2}}\,e^{-i\omega t}. \tag{14}$$

Physically, Eq. (14) represents the reaction of the coupled system to the initial distribution of electrons, resulting in oscillations of the scalar potential. Later this can be expressed as the sum of all contributions: $\varphi_{\mathbf{k}} = \varphi^{R^+}_{\mathbf{k}} + \varphi^{R^-}_{\mathbf{k}} + \varphi^{\mathcal{C}}_k$, where $\varphi^{R^\pm}_{\mathbf{k}}$ is the pole contributions and $\varphi^{\mathcal{C}}_k$ is the branch cut(s) contribution.

The integrand of Eq. (14) can be analytically continued to the lower half plane of complex ω as discussed above. For this we choose the BC-I. Using the residue theorem, the pole contribution to the potential reads

$$\varphi^{R^+}_{\mathbf{k}}(t) + \varphi^{R^-}_{\mathbf{k}}(t) \equiv \sum_l \frac{\left(\omega_l^2-\omega^2_{\rm TO}+i\gamma_{\rm TO}\omega_l\right)e^{-i\omega_l t}}{\partial\varepsilon(\omega,k)/\partial\omega|_{\omega=\omega_l}\sqrt{\omega_l^2-v_F^2k^2}}, \tag{15}$$

where the summation is running over all existing poles, which arise for the branches $\omega^\pm$, taking into account also negative ω'. The branch cut contribution reads

$$\varphi^{\mathcal{C}}_k(t) = \frac{k}{\pi}\int_{-v_Fk}^{v_Fk} d\omega\,\frac{\sqrt{v_F^2k^2-\omega^2}[K+k(1+\overline{\Omega})]e^{-i\omega t}}{\left(v_F^2k^2-\omega^2\right)[K+k(1+\overline{\Omega})]^2+\omega^2K^2}, \tag{16}$$

where $K = e^2gk_BT\ln[\exp(E_F/k_BT)+1]/(\kappa^*_\infty\hbar^2v_F^2)$, and $\overline{\Omega} = (\omega^2_{\rm TO}-\omega^2_{\rm SO})/(\omega^2-\omega^2_{\rm TO}+i\gamma_{\rm TO}\omega)$. Note that the square root in Eq. (16) is a simple algebraic function, where ω and k are real. In the long wavelength limit, or in the case of weak coupling, the simplified expressions for Eq. (16) can be found in Ref. [12]. In the case of strong coupling and $v_Fkt \gg 1$, $\varphi^{\mathcal{C}}_k$ oscillates with frequency v_Fk and decays in time according to the power law

$$\varphi^{\mathcal{C}}_k(t) = \sqrt{\frac{2}{\pi}}\frac{\left(\omega^2_{\rm TO}-v_F^2k^2\right)}{\left(\omega^2_{\rm SO}-\omega^2_{\rm TO}\right)}\frac{\sin\left(v_Fkt+\pi/4\right)}{(v_Fkt)^{1/2}}. \tag{17}$$

Figures 2(c)–2(e) show examples of the joint oscillations of coupled plasmon-SO phonon modes calculated using Eqs. (15) and (16), and their spectral amplitudes, obtained by the fast Fourier transform (FFT) for $v_Fk/\omega_{\rm TO} = 0.5$ and 0.8. The signal for $v_Fk/\omega_{\rm TO} = 0.5$ shown in Fig. 2(c) contains both coupled plasmon-SO phonon modes, as confirmed by the calculations of the spectral amplitudes presented in Fig. 2(e). Meanwhile, the signal for $v_Fk/\omega_{\rm TO} = 0.8$ in Fig. 2(d) looks almost harmonic, which is explained by the domination of oscillations with frequency ω_+, as seen in Fig. 2(e). Remarkably, the spectral amplitude of the ω_- mode rapidly decreases as curve $\omega_-(k)$ approaches the transverse optical phonon frequency, and eventually this mode disappears. We refer to this effect as mode *collapse*.

The line shape of the mode ω_+ is Lorentzian [41] and its spectral density is dominant in the signal. The mode ω_+ is the same for both chosen branch cuts. In this case the contribution $\varphi^-_k(t) \equiv \varphi^{R^-}_k(t) + \varphi^{\mathcal{C}}_k(t)$ remains unambiguous and independent of the choice of the branch cut(s). This allows us to exclude the pole contribution $\varphi^{R^+}_k$ from the signal for better visualization of the results.

The spectral FFT amplitudes of the signals $\varphi^-_k(t)$ are shown in Fig. 3 for the different values of v_Fk. One can see how this spectral amplitude collapses with increasing of k. Only weak traces of the ω_- oscillations can be seen in the A-II and A-III regions of k, where the dispersion relation does predict relevant oscillations [see Figs. 2(a) and 2(b)]. In the time-domain picture, the branch points contribute strongly at initial times, where signals decrease from their initial amplitude by $\sim$3.7 times at $v_Fk = 0.8\,\omega_{\rm TO}$ and by $\sim$16 times at $v_Fk = 1.3\,\omega_{\rm TO}$ (see insets to Fig. 3). For the frequency domain, these fast processes determine the visible background of the spectral amplitudes, as presented in Fig. 3 for $v_Fk/\omega_{\rm TO} \geqslant 1$. Moreover, the branch points manifest themselves as a smeared spike at $\omega = v_Fk$.

Remarkably, the ω_- branch line shape is strongly asymmetric, like that for the Fano resonance [42,43]. Generally, the Fourier-Laplace components provide not only amplitudes of oscillations, but also their phases. Analyzing relevant phases, e.g., for the potential oscillations, we found their regular behavior for the ω_+ branch at any ω, k, while observed quite irregular changes of the phases for the ω_- branch in the regions of the collapse of these oscillations (see Ref. [37] for details).

Physics explaining the collapse effect lies in special features of dynamic screening by Dirac electrons. Indeed, Dirac electrons strongly screen space-time-dependent electrical fields at frequencies of the order of v_Fk [44]. Since the optical displacement $\mathbf{w}_{\omega,\mathbf{k}}$ and the lattice polarization $\mathbf{P}_{\omega,\mathbf{k}}$ are proportional to the electric field $\mathbf{E}_{\omega,\mathbf{k}}$, the screening of the field suppresses the coupled oscillations.

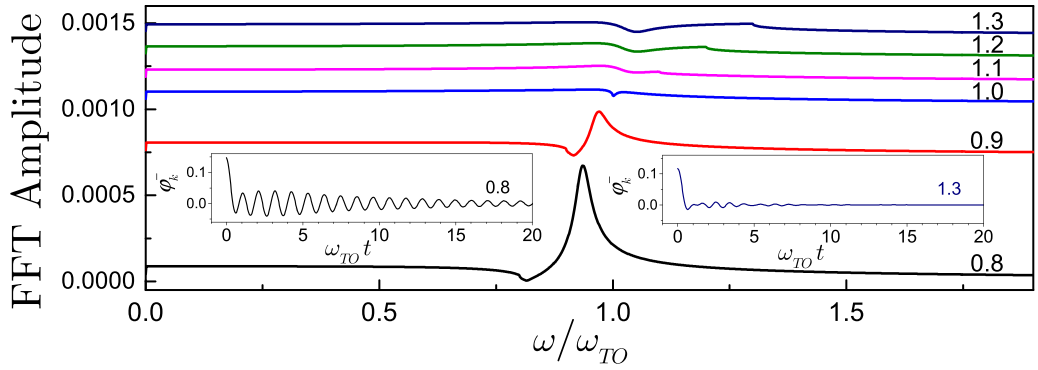


FIG. 3. Spectral FFT amplitudes of the signals $\varphi_k^-(t)$ for the different values of $v_F k$ from $0.8\,\omega_{\rm TO}$ to $1.3\,\omega_{\rm TO}$. The insets show examples of the signals at $v_F k = 0.8\,\omega_{\rm TO}$ (left) and $v_F k = 1.3\,\omega_{\rm TO}$ (right), respectively.

The experimental evidence of the collapse effect can be seen in the results of Refs. [14,15], where authors used high-resolution electron-energy-loss spectroscopy to investigate the coupled plasmon-SO phonon modes. The authors demonstrate that as the ω_- branch approaches the line $\omega = \omega_{\rm TO}$, the error bars of the data significantly increase, which indicates the difficulties in determining the spectral position of $\omega_-(k)$. In the same time, the ω_+ branch is much more visible until large values of k (see Fig. 2 in Ref. [14]). Moreover, while mode ω_+ is well visible in the intensity, mode ω_- is hardly visible (see Fig. 1(b) in Ref. [15]), which indicates the effect of collapse.

To conclude, in theories of collective excitations and waves the important role is assigned to the dispersion equation, which relates the frequency and wave number of the excitations. However, if this dispersion equation contains branch points, the dispersion equation approach can give ambiguous solutions. In such cases the physical picture of excitations becomes uncertain. Correct results can be obtained by solving, for example, an initial value problem, which leads to an unambiguous solution that does not depend on the choice of branch cut(s) [45].

To demonstrate this, we considered strong coupling between plasmons of graphene and surface optical phonons of a polar substrate. We showed that solutions of the dispersion equation essentially depend on the branch cuts on the ω plane. To clarify the character of the coupled oscillations, we solved a relevant initial value problem and defined the full physical picture of these oscillations. Particularly, we found that lower plasmon-phonon mode ω_-, which in terms of the dispersion equation can have a good quality factor, is almost absent in the excitation spectra. The main physical reason for this collapse is the suppression of space-time-dependent electric fields near $\omega = v_F k$.

Note that multivalued dispersion equations can be found for various problems. For instance, the dispersion equation for surface-plasmon polaritons (see, e.g., Ref. [46]) contains square root branching. Branch points also arise in acoustics [47,48], plasma physics [49], Bose-Einstein condensate [50], the branch cut cosmology [51], the theory of neutrino [52], etc. Our findings indicate that mathematically correct handling of multivalued dispersion equations facilitates understanding the relevant physical picture, including possible new effects.

We are grateful to Maksym Strikha for the fruitful discussions during the early stages of this work. We acknowledge the long-term program of support of the Ukrainian research teams at the Polish Academy of Sciences carried out in collaboration with the U.S. National Academy of Sciences with the financial support of external partners, Project LTP NAS KOCHELAP A7.11.0008. S.M.K. acknowledges the partial support of the National Research Foundation of Ukraine, Project No. 2023.05/0022.

[1] L. D. Landau and E. M. Lifshits, *Course of Theoretical Physics: Physical Kinetics* (Pergamon, New York, 1981), Vol. 10.
[2] S. A. Maier, *Plasmonics: Fundamentals and Applications* (Springer, New York, 2007).
[3] G. Giuliani and G. Vignale, *Quantum Theory of the Electron Liquid* (Cambridge University Press, New York, 2008).
[4] V. V. Mitin, V. A. Kochelap, and M. A. Stroscio, *Quantum Heterostructures: Microelectronics and Optoelectronics* (Cambridge University Press, New York, 1999).
[5] V. V. Mitin, V. A. Kochelap, M. Dutta, and M. A. Stroscio, *Introduction to Optical and Optoelectronic Properties of Nanostructures* (Cambridge University Press, New York, 2019).
[6] J. M. D. Coey, *Magnetism and Magnetic Materials* (Cambridge University Press, New York, 2010).
[7] A. Rahimi-Iman, *Fundamentals of Polariton Physics* (Springer, Cham, 2020), Vol. 229.
[8] L. D. Landau, On the vibrations of the electronic plasma, Akad. Nauk SSSR. Zhurnal Eksper. Teoret. Fiz. **16**, 574 (1946) [Acad. Sci. USSR. J. Phys. **10**, 25 (1946)].
[9] B. Wunsch, T. Stauber, F. Sols, and F. Guinea, Dynamical polarization of graphene at finite doping, New J. Phys. **8**, 318 (2006).
[10] E. H. Hwang and S. Das Sarma, Dielectric function, screening, and plasmons in two-dimensional graphene, Phys. Rev. B **75**, 205418 (2007).
[11] A. H. Castro Neto, F. Guinea, N. M. R. Peres, K. S. Novoselov, and A. K. Geim, The electronic properties of graphene, Rev. Mod. Phys. **81**, 109 (2009).
[12] S. M. Kukhtaruk and V. A. Kochelap, Semiclassical analysis of intraband collective excitations in a two-dimensional electron gas with Dirac spectrum, Phys. Rev. B **92**, 041409(R) (2015).

[13] É. de Mello Silva, Dynamical class of a two-dimensional plasmonic Dirac system, Phys. Rev. E **92**, 042146 (2015).
[14] R. J. Koch, Th. Seyller, and J. A. Schaefer, Strong phonon-plasmon coupled modes in the graphene/silicon carbide heterosystem, Phys. Rev. B **82**, 201413(R) (2010).
[15] R. J. Koch, T. Haensel, S. I.-U. Ahmed, Th. Seyller, and J. A. Schaefer, HREELS study of graphene formed on hexagonal silicon carbide, Phys. Status Solidi C **7**, 394 (2010).
[16] E. H. Hwang, R. Sensarma, and S. Das Sarma, Plasmon-phonon coupling in graphene, Phys. Rev. B **82**, 195406 (2010).
[17] M. Jablan, M. Soljacic, and H. Buljan, Unconventional plasmon-phonon coupling in graphene, Phys. Rev. B **83**, 161409(R) (2011).
[18] Z.-Y. Ong and M. V. Fischetti, Theory of interfacial plasmon-phonon scattering in supported graphene, Phys. Rev. B **86**, 165422 (2012).
[19] Z.-Y. Ong and M. V. Fischetti, Theory of remote phonon scattering in top-gated single-layer graphene, Phys. Rev. B **88**, 045405 (2013).
[20] E. H. Hwang and S. Das Sarma, Surface polar optical phonon interaction induced many-body effects and hot-electron relaxation in graphene, Phys. Rev. B **87**, 115432 (2013).
[21] Y. Liu, R. F. Willis, K. V. Emtsev, and Th. Seyller, Plasmon dispersion and damping in electrically isolated two-dimensional charge sheets, Phys. Rev. B **78**, 201403(R) (2008).
[22] J. Lu, K. P. Loh, H. Huang, W. Chen, and A. T. S. Wee, Plasmon dispersion on epitaxial graphene studied using high-resolution electron energy-loss spectroscopy, Phys. Rev. B **80**, 113410 (2009).
[23] Y. Liu and R. F. Willis, Plasmon-phonon strongly coupled mode in epitaxial graphene, Phys. Rev. B **81**, 081406(R) (2010).
[24] T. Langer, J. Baringhaus, H. Pfnür, H. W. Schumacher, and C. Tegenkamp, Plasmon damping below the Landau regime: The role of defects in epitaxial graphene, New J. Phys. **12**, 033017 (2010).
[25] C. Tegenkamp, H. Pfnür, T. Langer, J. Baringhaus, and H. W. Schumacher, Plasmon electron-hole resonance in epitaxial graphene, J. Phys.: Condens. Matter **23**, 012001 (2011).
[26] M. Freitag, T. Low, W. Zhu, H. Yan, F. Xia, and P. Avouris, Photocurrent in graphene harnessed by tunable intrinsic plasmons, Nat. Commun. **4**, 1951 (2013).
[27] F. J. Bezares, A. De Sanctis, J. R. M. Saavedra, A. Woessner, P. Alonso-González, I. Amenabar, J. Chen, T. H. Bointon, S. Dai, M. M. Fogler, D. N. Basov, R. Hillenbrand, M. F. Craciun, F. J. García de Abajo, S. Russo, and F. H. L. Koppens, Intrinsic plasmon–phonon interactions in highly doped graphene: A near-field imaging study, Nano Lett. **17**, 5908 (2017).
[28] A. N. Grigorenko, M. Polini, and K. S. Novoselov, Graphene plasmonics, Nat. Photonics **6**, 749 (2012).
[29] S. Xiao, X. Zhu, B.-H. Li, and N. A. Mortensen, Graphene-plasmon polaritons: From fundamental properties to potential applications, Front. Phys. **11**, 117801 (2016).
[30] S. Huang, C. Song, G. Zhang, and H. Yan, Graphene plasmonics: Physics and potential applications, Nanophotonics **6**, 1191 (2017).
[31] S. Ogawa, S. Fukushima, and M. Shimatani, Graphene plasmonics in sensor applications: A review, Sensors **20**, 3563 (2020).
[32] D. T. Nurrohman and N.-F. Chiu, A review of graphene-based surface plasmon resonance and surface-enhanced raman scattering biosensors: Current status and future prospects, Nanomaterials **11**, 216 (2021).
[33] L. Cui, J. Wang, and M. Sun, Graphene plasmon for optoelectronics, Rev. Phys. **6**, 100054 (2021).
[34] Hereafter, we use similar representation for any 3D vector, i.e., $\mathbf{V} = (\mathbf{V}_\parallel, V_z)$.
[35] M. Born and K. Huang, *Dynamical Theory of Crystal Lattices* (Clarendon, Oxford, 1954).
[36] P. M. Morse and H. Feshbach, *Methods of Theoretical Physics* (McGraw-Hill, New York, 1953), Parts I and II.
[37] See Supplemental Material at http://link.aps.org/supplemental/10.1103/PhysRevB.110.L241403 for details of substrate polarization and boundary conditions, surface optical phonons, analytical continuation and Fourier analysis of the signals.
[38] S. Fratini and F. Guinea, Substrate-limited electron dynamics in graphene, Phys. Rev. B **77**, 195415 (2008).
[39] N. G. van Kampen, On the theory of stationary waves in plasmas, Physica **21**, 949 (1955).
[40] W. Norimatsu, A review on carrier mobilities of epitaxial graphene on silicon carbide, Materials **16**, 7668 (2023).
[41] One must consider the square of amplitudes (power) to discuss line shapes. However, in this case, the ω_- line will be almost invisible near $\omega = v_F k$, therefore we will focus on the amplitudes.
[42] Y. S. Joe, A. M. Satanin, and C. S. Kim, Classical analogy of Fano resonances, Phys. Scr. **74**, 259 (2006).
[43] A. E. Miroshnichenko, S. Flach, and Y. S. Kivshar, Fano resonances in nanoscale structures, Rev. Mod. Phys. **82**, 2257 (2010).
[44] S. M. Kukhtaruk, V. A. Kochelap, V. N. Sokolov, and K. W. Kim, Spatially dispersive dynamical response of hot carriers in doped graphene, Physica E **79**, 26 (2016).
[45] Another possible way is to formulate the boundary value problem.
[46] J. M. Pitarke, V. M. Silkin, E. V. Chulkov, and P. M. Echenique, Theory of surface plasmons and surface-plasmon polaritons, Rep. Prog. Phys. **70**, 1 (2007).
[47] L. Tsang, Time-harmonic solution of the elastic head wave problem incorporating the influence of Rayleigh poles, J. Acoust Soc. Am. **63**, 1302 (1978).
[48] V. Gusev, C. Desmet, W. Lauriks, C. Glorieux, and J. Thoen, Theory of Scholte, leaky Rayleigh, and lateral wave excitation via the laser-induced thermoelastic effect, J. Acoust. Soc. Am. **100**, 1514 (1996).
[49] T.-X. Hu, Dong Wu, Z. M. Sheng, and J. Zhang, Exact dispersion relation of the quantum Langmuir wave, Phys. Rev. E **109**, 065213 (2024).
[50] L. M. Farrell, C. J. Howls, and D. H. J. O'Dell, Logarithmic catastrophes and Stokes's phenomenon in waves at horizons, J. Phys. A: Math. Theor. **56**, 044001 (2023).
[51] C. A. Zen Vasconcellos, P. O. Hess, J. de Freitas Pacheco, D. Hadjimichef, and B. Bodmann, The branch-cut cosmology: evidences and open questions, Astron. Nachr. **344**, e220079 (2023).
[52] D. F. G. Fiorillo and G. G. Raffelt, Theory of neutrino fast flavor evolution. Part I. Linear response theory and stability conditions, J. High Energy Phys. 08 (2024) 225.